

Spaceborne SAR Data for Global Urban Mapping at 30m Resolution

UtilizingUsing a Robust Urban Extractor

Yifang Ban¹, Alexander Jacob¹ and Paolo Gamba²

1. KTH Royal Institute of Technology, Stockholm, Sweden
2. University of Pavia, Pavia, Italy

Abstract

With more than half of the world population now living in cities and 1.4 billion more people expected to move into cities by 2030, urban areas pose significant challenges on local, regional and global environment. Timely and accurate information on spatial distributions and temporal changes of urban areas are therefore needed to support sustainable development and environmental change research. The objective of this research is to evaluate spaceborne SAR data for improved global urban mapping using a robust processing chain, the KTH-Pavia Urban Extractor. ~~ENVISAT ASAR C-VV data at 30m resolution were selected over 10 global cities from six continents.~~ The proposed processing chain includes urban extraction based on spatial indices and Grey Level Co-occurrence Matrix (GLCM) textures, an existing method and several improvements i.e., SAR data preprocessing, enhancement, ~~urban extraction based on spatial indices and GLCM textures,~~ and post-processing. ENVISAT Advanced Synthetic Aperture Radar (ASAR) C-VV data at 30m resolution were selected over 10 global cities and a rural area from six continents to demonstrated robustness of the improved method. The results show that the KTH-Pavia Urban Extractor is effective in extracting urban areas and small towns from ENVISAT ASAR data and urban-built-up areas can be mapped at 30m resolution with very good accuracy using only one or two SAR images. These findings indicate that operational global

1
2
3
4
5
6
7
8
9
10
11
12
13
14
15
16
17
18
19
20
21
22
23
24
25
26
27
28
29
30
31
32
33
34
35
36
37
38
39
40
41
42
43
44
45
46
47
48
49
50
51
52
53
54
55
56
57
58
59
60
61
62
63
64
65

urban mapping is possible with spaceborne SAR data, especially with the launch of Sentinel-1 that provides SAR data with global coverage, operational reliability and quick data delivery.

Keywords:

Spaceborne SAR, ENVISAT ASAR, Urban Mapping, 30m Resolution, Spatial Indices, GLCM Textures, Mountain Mask

1. Introduction

In 2008, the world crossed an invisible but momentous milestone - more than half of the people on the planet - roughly 3.2 billion human beings - lived in cities. It is estimated that the world is expected to add an additional 1.4 billion urban dwellers by 2030, and by 2050, approximately 67% of the world population is expected to live in cities (UN 2011). Although only a small percentage of global land cover, urban areas significantly alter climate, biogeochemistry, and hydrology at local, regional, and global scales (Seto *et al.*, 2011). Cities are hot spots of production, consumption, and waste generation. According to the United Nations, cities are responsible for 75% of global energy consumption and 80% of greenhouse gas emissions (Ash *et al.*, 2008). The impact of urban areas on atmospheric chemistry and aerosols is both pronounced and well-documented. Urban land use influences local to regional climates through urban heat islands, impervious surfaces alter sensible and latent heat fluxes, and recent evidence has suggested that cities may also significantly affect precipitation regimes (Schneider *et al.*, 2009). Therefore, timely and reliable information on the spatial distribution and the temporal changes of urban areas is therefore critical to a wide array of research questions related to the effect of humans on the local, regional and global environment (Schneider *et al.*, 2009) as well as to support sustainable urban development.

1
2
3
4
5
6
7
8
9
10
11
12
13
14
15
16
17
18
19
20
21
22
23
24
25
26
27
28
29
30
31
32
33
34
35
36
37
38
39
40
41
42
43
44
45
46
47
48
49
50
51
52
53
54
55
56
57
58
59
60
61
62
63
64
65

With its synoptic view and the repeatability, satellite remote sensing has been extensively used for urban mapping and monitoring. During the last two decades, eight different teams have developed 10 global land cover maps that offer circa-2000 portraits of urban areas (Gamba and Herold, 2009; Potere *et al.*, 2009; Schneider *et al.*, 2010). Based on the extensive assessments conducted by Potere *et al.* (2009) and Schneider *et al.* (2010), the new MODIS 500 m resolution global urban map has the highest accuracy among all global urban maps at coarse resolution. The MODIS classification approach employed a one-year time series of seven land bands MODIS data to exploit spectral and temporal properties of land cover types and to reduce the effect of the missing data due to cloud cover.

Previous global land cover products derived using time series optical satellite data at coarse spatial resolution (300m–1km), however, did not provide sufficient thematic detail or change information for global change studies and for resource management. High resolution (~30 m) land cover characterization and monitoring is needed that permits detection of land change at the scale of most human activity and offers the increased flexibility of environmental model parameterization needed for global change studies. However, there are a number of challenges to overcome before producing such data sets including unavailability of consistent global coverage of satellite data, sheer volume of data, unavailability of timely and accurate training and validation data, difficulties in preparing image mosaics, and high performance computing requirements (Giri *et al.*, 2013). In spite of these difficulties, China recently produced a 30m global land cover map using Landsat data with a promising overall accuracy of 65% (Gong *et al.*, 2013). For the 2010 classification, however, 74% of all Landsat data were from 2006 to 2011 and majority of the data were from non-summer season. Several classes including impervious areas were poorly classified. Some of the accuracies for impervious lands fall below 20%.with a

1
2
3
4
5
6
7
8
9
10
11
12
13
14
15
16
17
18
19
20
21
22
23
24
25
26
27
28
29
30
31
32
33
34
35
36
37
38
39
40
41
42
43
44
45
46
47
48
49
50
51
52
53
54
55
56
57
58
59
60
61
62
63
64
65

barely 10.5% producer’s accuracy and 30.8% user’s accuracy (Gong *et al.*, 2013). These results clearly call for further research and development to improve global urban mapping at 30m resolution.

Current trends in global land-cover classification have shifted from a single general purpose land cover classification to individual class information extraction such as human settlements (e.g., Schneider *et al.*, 2010; Gamba and Lisini, 2013), agricultural lands (e.g., Thenkabail *et al.*, 2009), wetlands (e.g., Giri *et al.*, 2010) and forest cover (e.g., Townshend *et al.*, 2012) among others (Gong *et al.*, 2013). Urban extent and land cover have been mapped using a range of datasets and algorithms (Gamba and Herold, 2009). Very High Resolution optical and/or SAR imagery and object-based approaches dominate urban remote sensing at the local level (e.g., Gong *et al.*, 1992; Jacquin *et al.*, 2003; Ban *et al.*, 2010; Moran, 2010; Gamba *et al.*, 2011; Niu and Ban, 2013) while Landsat, ENVISAT ASAR, MERIS as well as MODIS or nighttime light data and pixel-based techniques are mostly used for regional and global analysis (e.g., Lu *et al.*, 2008; Elvidge *et al.*, 2009; [Esch *et al.*, 2010](#); Arino, *et al.*, 2010; Friedl *et al.*, 2010; Schneider *et al.*, 2010; Wang *et al.* 2010; Zhang and Seto, 2011, Chen *et al.*, 2012; Taubenböck *et al.* 2012; Wang, *et al.*, 2012; Gamba and Lisini, 2013; [Angiuli & Trianni, 2014](#)). One of the recent developments are moving towards global urban extraction using optical data at very high spatial resolution. For examples, Pesaresi *et al.* (2011) developed a texture-based algorithm to extract urban extent of over 40 cities around the globe using Ikonos and QuickBird panchromatic data resampled to a nominal resolution at 10 m. [Kemper *et al.* \(2013\) presented a general framework for processing high and very high resolution data in support to a Global Human Settlement Layer \(GHSL\) and the resolution of the input images ranges from 0.5 to 10 meters, collected by a heterogeneous set of platforms including satellite SPOT \(2 and 5\), CBERS 2B, RapidEye \(2 and 4\), WorldView \(1 and](#)

1
2
3
4
5
6
7
8
9
10
11
12
13
14
15
16
17
18
19
20
21
22
23
24
25
26
27
28
29
30
31
32
33
34
35
36
37
38
39
40
41
42
43
44
45
46
47
48
49
50
51
52
53
54
55
56
57
58
59
60
61
62
63
64
65

2). GeoEye 1, QuickBird 2, Ikonos 2, and airborne sensors. The framework and techniques are promising, but true global mapping with such data remains a challenge due to the huge amount of data and computations involved as well as data availability issue due to cloud cover. Compared to optical data, SAR data have not been equally explored in urban applications due to the complexity of their interactions with diverse urban features. With its all-weather/illumination capability and its unique information content, however, SAR data have been increasingly investigated for global urban extent extraction at various spatial resolutions with promising results. For examples, Gamba *et al.* (2011) developed a method to extract global urban area extent from SAR images. The proposed approach utilizes a group of spatial indices, i.e., Moran's, Geary's, and Getis' together with GLCM-based textures (i.e., correlation and variance) for urban extent extraction. The method has been tested in different set of SAR images produced using different sensors (e.g., POLSAR, RADARSAT-1, TerraSAR-X, COSMO/SkyMed, etc.), with different spatial resolutions that cover different cities around the world with promising results. Esch *et al.* (2012 and 2013), on the other hand, developed a method to extract global urban settlement from TanDEM-X images at 12m spatial resolution. The method consists of three main steps: (1) textural information extraction that can be used to highlight built-up areas; (2) unsupervised classification of built-up/non built-up areas that takes into account both backscattered amplitude and the extracted textural information; (3) a final step that focuses on post-processing and mosaicking to produce a final urban map. The proposed methodology was evaluated using images that cover New Delhi, Munich, Buenos Aires, Nairobi, and Padang with an overall accuracy up to 94.8% achieved. On-going efforts are currently undertaken to produce a consistent global map of human settlements at a few meters' spatial resolution, but the final results are yet to be achieved. Even when these maps are released, it is still desirable to develop method for urban extraction using ENVISAT ASAR or ERS-1/-2 data since ENVISAT ASAR

1
2
3
4
5
6
7
8
9
10
11
12
13
14
15
16
17
18
19
20
21
22
23
24
25
26
27
28
29
30
31
32
33
34
35
36
37
38
39
40
41
42
43
44
45
46
47
48
49
50
51
52
53
54
55
56
57
58
59
60
61
62
63
64
65

and ERS-1/-2 data could provide global urban maps from earlier time when TerraSAR-X or TanDEM-X data were not available.

As a compromise between the spatial details and the amount of data and computation, Gamba and Lisini (2013) developed an efficient method for urban areas extraction using ENVISAT ASAR wide swath mode at 75m resolution aiming to improve GlobCover 2009 urban mapping results. The method consists of three phases: (1) preprocessing, i.e., multitemporal images filtering, averaging, and equalization; (2) urban extraction, i.e., seed extraction and region growing; (3) post-processing, i.e., DEM-based correction, hole filling, and aggregation to 300m spatial resolution. Test areas from around the world were used to evaluate the efficiency of the proposed approach and overall accuracies up to 94.8% were achieved using validation data of 1000 randomly selected points. The results are very encouraging, but the method requires a large volume of multitemporal SAR data (10-50 images) as the algorithm is based on amplitude values only, thus the denser the time series data, the better the accuracy. The above literature analysis indicates a strong need of robust and operational methods for global urban extraction using a small number of SAR images at medium resolution. Therefore, the objective of this research is to evaluate ENVISAT SAR data at 30m resolution for improved global urban mapping using a robust processing chain, the KTH-Pavia Urban Extractor, an improved method based on Gamba et al. (2011).

2. Study Areas and Data Description

Ten cities around the world were selected to represent developed and developing cities in various environmental conditions in all continents except Antarctica (Fig. 1). Coastal cities include Jakarta, Lagos, Mumbai, New York, Rio de Janeiro, Stockholm, and Sydney while inland cities

1
2
3
4
5
6
7
8
9
10
11
12
13
14
15
16
17
18
19
20
21
22
23
24
25
26
27
28
29
30
31
32
33
34
35
36
37
38
39
40
41
42
43
44
45
46
47
48
49
50
51
52
53
54
55
56
57
58
59
60
61
62
63
64
65

include Beijing, Berlin, and Mexico City. Several cities are mountainous or surrounded by mountains while the rest are in relatively flat areas. Some of the cities are under rapid urbanization while others grow relatively slowly. In addition to the ten big cities, Lombardia in Northern Italy was also selected to evaluate the effective of the KTH-Pavia Urban Extrator for extracting smaller towns.

ENVISAT ASAR data were selected for all cities during the vegetation season to maximize the difference between urban and rural areas. Ideally, multi-date, dual polarization data from both ascending and descending orbit are needed to evaluate the potential of ENVISAT ASAR data for improved urban extraction. For most of the cities selected, however, only a single date, single-polarization C-VV SAR data were available. Beijing is the only city with multitemporal SAR data ~~multitemporal, in~~ alternating polarization and dual orbits available in early vegetation season. With the launch of Sentinel-1 ~~in-on April 3, 2014-and the planned RADARSAT constellation missions~~, spaceborne SAR data with global coverage, operational reliability and quick data delivery will ~~become~~ be routinely available. They provide excellent opportunity for operational global urban mapping and monitoring. The detailed information of the ENVISAT ASAR data used in this research is ~~listed-presented~~ in Table 1.

To perform rigorous assessment of the urban mapping, validation data of urban and non-urban areas were randomly collected and evenly distributed throughout the image based on very high resolution Google images. The validation data consists of small rectangle blocks at approximately 50 pixels each and 10000 pixels in total for urban and non-urban areas respectively.

1
2
3
4
5
6
7
8
9
10
11
12
13
14
15
16
17
18
19
20
21
22
23
24
25
26
27
28
29
30
31
32
33
34
35
36
37
38
39
40
41
42
43
44
45
46
47
48
49
50
51
52
53
54
55
56
57
58
59
60
61
62
63
64
65



Figure 1. Study Areas

Table 1. ENVISAT ASAR Data Characteristics

City	Acquisition Date	Mode	Orbit	Incidence Angles
Beijing	2009-05-17	AP, IS2	Ascending	19.2 - 26.7°
	2009-05-27	AP, IS2	Descending	19.2 - 26.7°
	2009-06-08	AP, IS4	Ascending	31.0 - 36.3°
	2009-06-11	AP, IS6	Ascending	39.1 - 42.8°
Berlin	2010-09-25	IM, IS2	Descending	19.2 - 26.7 °
Jakarta	2009-09-06	IM, IS2	Ascending	19.2 - 26.7°
Lagos	2010-08-18	IM, IS2	Descending	19.2 - 26.7°
Lombardia	<u>2010-07-20</u>	<u>IM, IS2</u>	<u>Ascending</u>	<u>19.2 - 26.7°</u>
	<u>2010-08-24</u>	<u>IM, IS2</u>	<u>Descending</u>	<u>19.2 - 26.7°</u>
Mexico City	2010-05-14	IM, IS2	Descending	19.2 - 26.7°
Mumbai	2010-06-27	IM, IS2	Descending	19.2 - 26.7°
New York	2010-07-26	IM, IS3	Ascending	26.0 – 31.4°
Rio de Janeiro	2010-01-15	IM, IS2	Ascending	19.2 - 26.7°
Stockholm	2006-06-16	IM, IS2	Descending	19.2 - 26.7°
Sydney	2010-09-03	IM, IS4	Descending	31.0 - 36.3°

3. Methodology

Due to speckle in SAR images, methodology for urban extraction from SAR needs to take into

1
2
3
4
5
6
7
8
9
10
11
12
13
14
15
16
17
18
19
20
21
22
23
24
25
26
27
28
29
30
31
32
33
34
35
36
37
38
39
40
41
42
43
44
45
46
47
48
49
50
51
52
53
54
55
56
57
58
59
60
61
62
63
64
65

account of the spatial relationships among pixels instead of using the intensity of a single pixel. As a result, texture measures and spatial indices were often employed and proven effective in urban extraction (e.g., Gamba and Stasolla, 2008, Gamba *et al.*, 2011; Esch *et al.*, 2012 and 2013), In this research, the proposed method is based on the original approach developed by Gamba *et al.* (2011) using both spatial indices and texture measures. The overview of the methodology in this research is illustrated in Figure 2 with the improvements highlighted in light and dark green. The improvements mainly involve preprocessing, enhancement, post-processing as well as decision level fusion using multitemporal and multipolarization data.

3.1 Preprocessing

All SAR data were corrected for relief displacement with SRTM using the Range Doppler algorithm using the NEST toolbox.

3.2 Contrast Enhancement

As contrast between urban and non-urban areas in an image is crucial for the methodology, all SAR images were enhanced using linear scaling. Since the SAR data are negatively skewed, a clip of 1% from the low end of the histogram and 4% from right end were performed with the 1% low values set to 0 and 4% high values set to 255. In the original procedure by Gamba *et al.*, the "normalization" procedure is embedded into the algorithm including the 2% clipping of the extremes. This could cause certain urban areas with very high backscatter being clipped away.

1
2
3
4
5
6
7
8
9
10
11
12
13
14
15
16
17
18
19
20
21
22
23
24
25
26
27
28
29
30
31
32
33
34
35
36
37
38
39
40
41
42
43
44
45
46
47
48
49
50
51
52
53
54
55
56
57
58
59
60
61
62
63
64
65

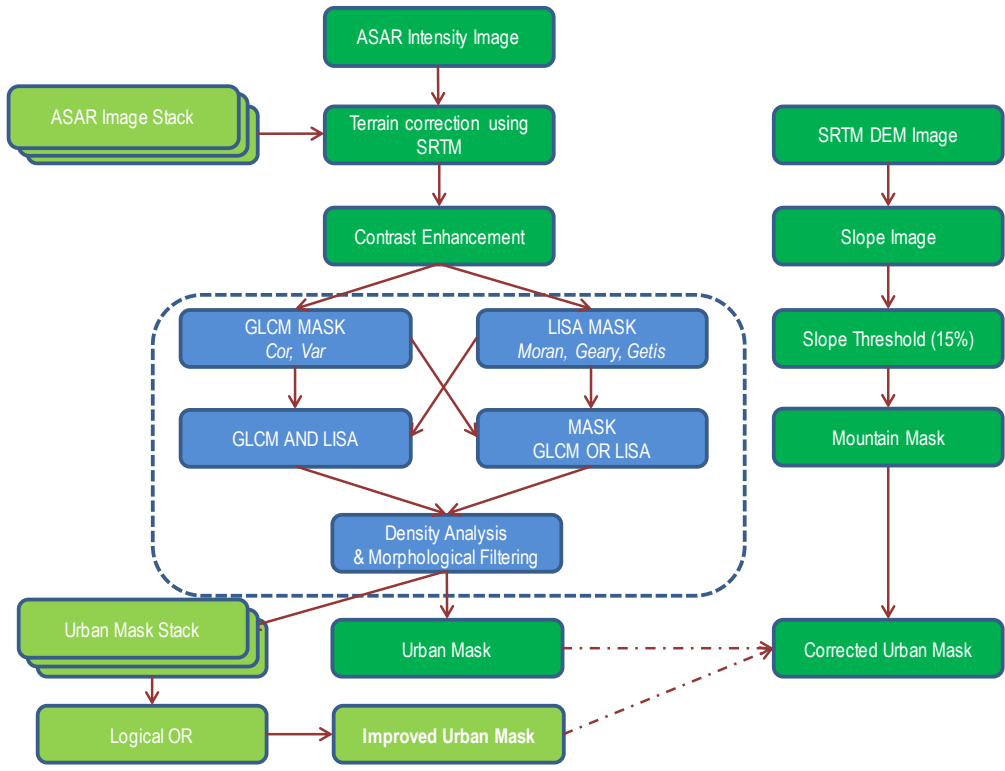


Fig. 2. Overview of the Methodology

In the same step, the SAR data were compressed from 16 bits to 8 bits to improve performance and reduce computation cost based on previous research. Clausi (2003), for example, suggests that there is no reason to compute GLCM on more than 8 bits in SAR images as more bits would include a lot of variability that is not captured by the textural measures, thus do not bring to any advantage on the following statistical analyses (e.g., a classification) of the GLCM features. In addition, using 16 bits the computation of the textural features is more than four times slower. The subsequent urban extraction process will be much slower too.

1
2
3
4
5
6
7
8
9
10
11
12
13
14
15
16
17
18
19
20
21
22
23
24
25
26
27
28
29
30
31
32
33
34
35
36
37
38
39
40
41
42
43
44
45
46
47
48
49
50
51
52
53
54
55
56
57
58
59
60
61
62
63
64
65

3.3 Urban Extraction using Spatial Indices and GLCM Texture

The method is based on “Local Indicators of Spatial Association” (L.I.S.A.), including the Moran index, the Geary index and the Getis-Ord index and GLCM variance and correlation textures as detailed in Gamba et al., 2011. For completeness of understanding, the indices and the GLCM textures are briefly explained below.

Moran’s I_i index: I_i evaluates the similarity between the neighbors of a pixel by comparing its value with the average local value. As a result, it describes local homogeneity by means of the following formula (where x_i is the generic pixel value at the i -th position):

$$I_i = \frac{x_i - \bar{x}}{\sum_i \frac{(x_i - \bar{x})^2}{n}} \sum_j w_{ij} (x_j - \bar{x}) \tag{1}$$

Please note that $I_i \in [-1, 1]$ and its value increases from negative to positive correlation.

Geary’s c_i index: c_i identifies areas of high contrast, providing a measure of local dissimilarity, according to

$$c_i = \frac{1}{\sum_i \frac{(x_i - \bar{x})^2}{n}} \sum_j w_{ij} (x_i - x_j)^2 \tag{2}$$

$c_i \in [1, 2]$ and the upper limit refers to strong negative spatial correlation, while the lower one corresponds to uncorrelated data.

Getis-Ord G_i index: G_i is useful to identify “outliers”, i.e., values very different from the surroundings:

$$G_i = \frac{\sum_j w_{ij} x_j}{\sum_j x_j}, \quad j \neq i. \quad (3)$$

The GLCM textures were computed with a moving window with a size of 11 x 11. Variance (VAR) and Correlation (COR) textures were chosen based on trials. Instead of 2% clipping of both left and right histogram tails implemented by Gamba et al. (2011), the contrast enhancement described in section 3.2 was used. In the approach, the COR and VAR textures are summed pixel by pixel into a unique image for urban extraction.

Based on the above indices and GLCM texture, LISA and/or GLCM masks were created and then processed through density analysis and morphological filtering to extract urban areas. In particular, the thresholds need to be determined for each satellite sensor accordingly in order to optimize for the specific characteristics of every sensor in terms of its spatial resolution and speckle behavior. The details are described in Gamba et al. (2011). The density is determined by the ratio of seed pixels per blob size. If this ratio is below the given threshold, the blob is filtered out. In this experiment, the following threshold settings were used: Scale Lisa 0.4, Scale Texture 0.1, Scale Urban 0.7, L.I.S.A Binarization 0.4 and Texture Binarization 0.7.

3.4 Mountain Masking

In SAR images, mountains facing the SAR have high backscatter similar to urban areas. In order to reduce the false positive due to mountainous areas, a simple step using a SRTM DEM is adopted based on Gamba and Lisini (2013). First, the 90m resolution SRTM DEM was resampled to 30m SAR resolution. Then the average slope is computed in a window around the pixel under test. If the slope value is ~~too~~ larger than 15°, an empirically determined value, ~~then~~ it

1
2
3
4
5
6
7
8
9
10 is highly likely that the high backscattering area is due to rocks and not urban. As a result, areas
11 where the average slope is higher than ~~an empirically determined value~~ (15°) are removed from
12 urban extraction.
13
14

15 16 17 18 3.5 Multitemporal Multi-Polarization Fusion

19 For the multitemporal alternating polarization and dual orbital data from Beijing, each SAR
20 image was processed by the procedures 3.1 to 3.4 to generate individual urban mask. Then these
21 urban masks were combined using simple logical operators such as AND or OR. In this research,
22 OR operator was used as all urban extraction results showed higher omission errors and low
23 commission errors.
24
25
26
27
28
29

30 31 3.6 Accuracy Assessment

32 To validate the urban extraction results, standard accuracy measures such as overall accuracy,
33 kappa, omission error and commission error were computed for results from KTH-Pavia Urban
34 Extractor, MODIS 500m and GlobCover using the validation 20 000 pixels as described earlier.
35
36

37 Omission errors occur when urban structures were not detected by the Urban Extractor.
38
39 Commission errors occur when the non-urban structures were mis-detected as urban, for
40 example, mountains.
41
42
43
44

45 4. Results and Discussion

46 47 4.1 Comparison of KTH-Pavia Urban Extractions with MODIS 500m and GlobCover

48 The urban extraction results using the KTH-Pavia approach are presented in ~~Table 2 and~~ Figure 3
49 and in Table 2 with comparison to MODIS 500m and GlobCover. The results show that KTH-
50 Pavia Urban Extractor produced more consistent results for all cities with overall accuracies
51
52
53
54
55

1
2
3
4
5
6
7
8
9
10
11
12
13
14
15
16
17
18
19
20
21
22
23
24
25
26
27
28
29
30
31
32
33
34
35
36
37
38
39
40
41
42
43
44
45
46
47
48
49
50
51
52
53
54
55
56
57
58
59
60
61
62
63
64
65

ranging from 78% to 92% (kappa ~~from 0.56 to 0.83~~ average at 0.71) while results of MODIS 500m and GlobCover are highly inconsistent with poor urban detection for several cities such as Beijing, Jakarta and Lagos for MODIS 500m and Jakarta, Mexico City and Rio for GlobCover. The average accuracies of MODIS 500m and GlobCover are also much lower than that of KTH-Pavia, with kappa at 0.53 and 0.47 respectively. For majority of the cities, KTH-Pavia method yielded higher overall accuracies and kappa with significantly less commission errors and Omission errors ranging from 15% to 40%. The best results are achieved over Jakarta with kappa at 0.83 (OA92%) that is significantly higher than MODIS 500m and GlobCover. The worst result (Kappa 0.56, OA: 74%) is from Rio with the highest commission error (7%) and omission error (nearly 40%). The omission errors are mainly caused by low-density builtup areas with trees that were not detected while the commission errors are caused by confusion between urban and other land cover classes with high backscatter in SAR images.

To provide direct comparisons, the KTH-Pavia urban areas are overlaid with MODIS 500m and GlobCover urban maps in Figures 4 and 5. For Jakarta, KTH-Pavia method performed best in finding not only the city center but also many of the smaller suburbs both in the south-east and south-west of the city core. GlobCover is only able to detect the most central parts and misses out completely on more remote urban areas. MODIS 500m was able to detect some of the suburbs in the south-east but nothing in the south-west. For Lagos, KTH-Pavia provided a very accurate view of the urban areas where it probably benefits from the higher resolution and hence can better deal with problems due to heavy urban sprawl in the city/rural boundary areas. MODIS 500m showed the worst result, being only able to find the most central part of the city but missing detection of almost all suburbs, likely due to confusion between urban areas and bare fields. GlobCover underestimates the urban areas in general but also showed some difficulties resulting

1
2
3
4
5
6
7
8
9
10 in commission errors to the north-east of the city core. For Beijing, KTH-Pavia approach
11 produced the most accurate result, which is also reflected in the urban areas detected. It gives a
12 more differentiated view of the city in terms of leaving out large parks and is able to find more of
13 the smaller satellite towns around the city, even though quite some are missed out. MODIS
14 produced a good result in the central part of the city but completely missed the suburbs. Probably
15 due to large pixel size it is not able to deal accurately with the high frequency of change in land
16 cover types ~~on-over~~ limited space. GlobCover had similar issue as MODIS 500m. For
17 Stockholm, MODIS 500m shows some obvious errors especially in the city center probably due
18 to the water bodies present where it heavily underestimates the urban area but also in the low
19 density suburbs the detection rate is low. GlobCover shows the best result especially in the low
20 density buildup suburbs where KTH-Pavia sometimes underestimates the urban extent.
21
22
23
24
25
26
27
28
29
30
31
32

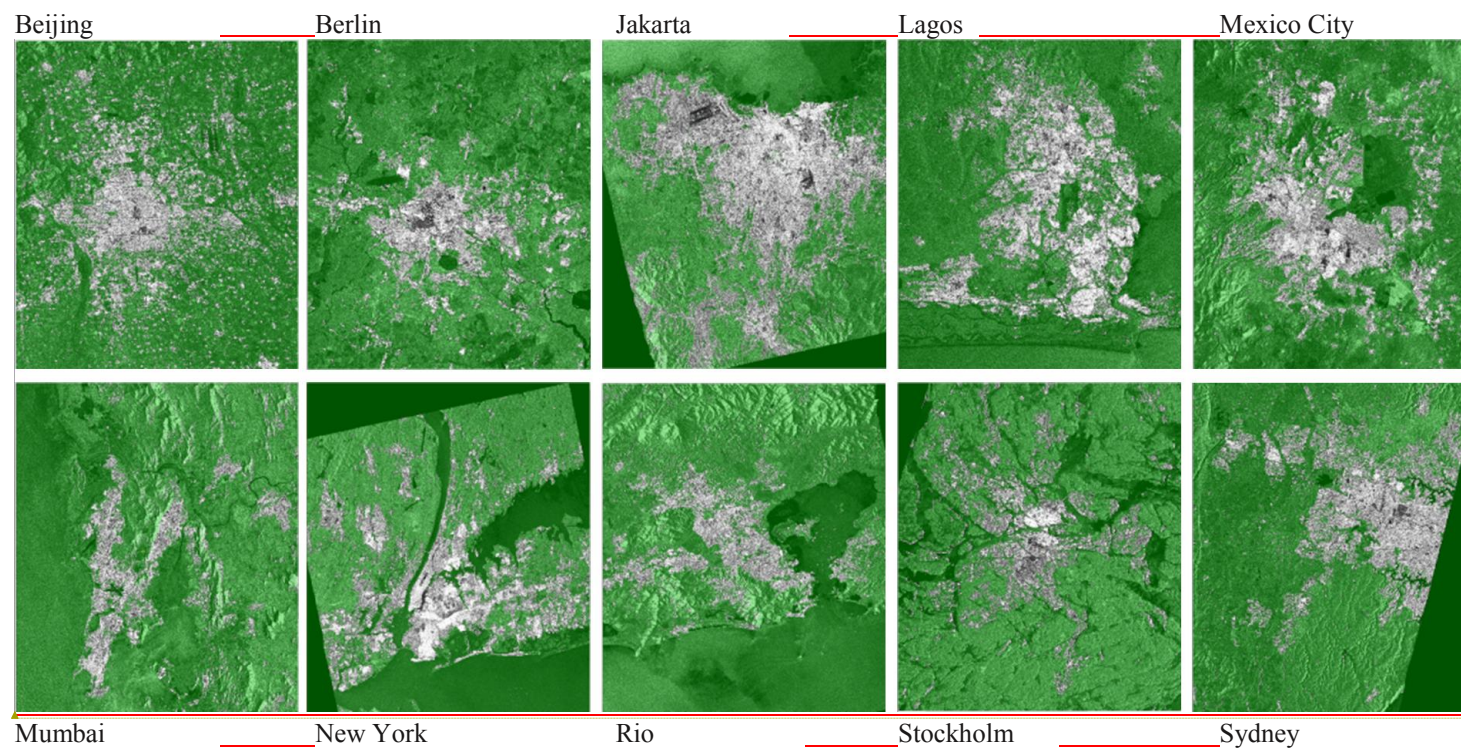
33 For the extraction of smaller towns, Table 3 shows that KTH-Pavia method using a single-date
34 ASAR in ascending orbit performed better than MODIS or GlobCover, but when applied the
35 method to the ASAR image in descending orbit, the accuracy is worse than MODIS or
36 GlobCover. The merge of the ascending and descending results improved the urban extraction
37 accuracy significantly and the accuracy (kappa: 0.83) is much higher than that of MODIS (kappa:
38 0.54) or GlobCover (kappa: 0.59). Figure 5 shows that KTH-Pavia method performed very well
39 for extraction of smaller towns while MODIS or GlobCover missed some built-up areas (in
40 yellow and blue) and over-estimated agricultural areas as urban areas (in green). These results
41 clearly show that KTH-Pavia Urban Extractor can be successfully used to extract both big cities
42 and smaller towns from 1-2 SAR images with reliable results.
43
44
45
46
47
48
49
50
51
52
53
54
55
56
57
58
59
60
61
62
63
64
65

Table 2. Accuracy Comparisons for KTH–Pavia Urban Extraction, MODIS 500m Global Urban Map and GlobCover 300m Global Urban Map

Cities	Urban Exctraction	Kappa	Overall Accuracy %	Urban Commission %	Urban Omission %
Beijing	KTH–Pavia	0,72	86	2,34	26,36
	<i>GlobCover</i>	0,71	85	12,56	17,48
	<i>MODIS 500m</i>	<i>0,45</i>	73	<i>27,62</i>	<i>27,02</i>
Berlin	KTH–Pavia	0,63	82	2,60	34,98
	<i>GlobCover</i>	0,71	85	12,56	17,48
	<i>MODIS 500m</i>	0,57	79	26,25	10,84
Jakarta	KTH–Pavia	0,83	92	3,06	15,15
	<i>GlobCover</i>	<i>0,17</i>	60	19,49	<i>79,17</i>
	<i>MODIS 500m</i>	<i>0,46</i>	74	9,24	<i>50,07</i>
Lagos	KTH–Pavia	0,66	83	0,00	33,41
	<i>GlobCover</i>	<i>0,38</i>	69	23,30	<i>44,36</i>
	<i>MODIS 500m</i>	<i>0,01</i>	50	47,03	<i>91,62</i>
Mexico City	KTH–Pavia	0,58	79	20,74	17,91
	<i>GlobCover</i>	<i>0,10</i>	53	23,71	<i>84,51</i>
	<i>MODIS 500m</i>	0,60	80	11,44	28,86
Mumbai	KTH–Pavia	0,74	87	2,14	23,03
	<i>GlobCover</i>	0,66	83	23,78	7,51
	<i>MODIS 500m</i>	0,74	87	10,84	17,53
New York City	KTH–Pavia	0,77	88	4,05	17,09
	<i>GlobCover</i>	0,57	70	0,88	38,83
	<i>MODIS 500m</i>	0,59	80	15,32	21,54
Rio de Janeiro	KTH–Pavia	0,56	78	7,02	39,84
	<i>GlobCover</i>	<i>0,20</i>	60	16,47	<i>75,34</i>
	MODIS 500m	0,67	83	21,98	7,75
Stockholm	KTH–Pavia	0,76	88	12,79	10,92
	GlobCover	0,83	92	7,41	9,90
	<i>MODIS 500m</i>	<i>0,54</i>	77	9,48	<i>40,22</i>
Sydney	KTH–Pavia	0,81	91	0,00	18,84
	<i>GlobCover</i>	<i>0,39</i>	69	<i>30,84</i>	<i>30,12</i>
	<i>MODIS 500m</i>	0,62	81	21,12	15,77
Average of 10 Cities	KTH–Pavia	0,71	85.4	5.47	23.75
	<i>GlobCover</i>	<i>0.47</i>	<i>72.6</i>	<i>17.1</i>	<i>40.47</i>
	<i>MODIS 500m</i>	<i>0.53</i>	<i>76.4</i>	<i>20.03</i>	<i>31.12</i>

Note: **Bold** represents the best accuracy for each city while *italic* shows the significantly worse accuracies.

1
2
3
4
5
6
7
8
9
10
11
12
13
14
15
16
17
18
19
20
21
22
23
24
25
26
27
28
29
30
31
32
33
34
35
36
37
38
39
40
41
42
43
44
45
46
47
48
49



Formatted: Font: (Default) Times
New Roman, Font color: Custom
Color(RGB(26,24,24))

Figure 3. **Comparisons of Urban Extractions Results in 10 Cities, White/Grey: Urban Areas; Green: Non-urban Areas. Top Row: KTH-Pavia method, Middle Row: GlobCover and Bottom Row: MODIS-500m**

1
2
3
4
5
6
7
8
9
10
11
12
13
14
15
16
17
18
19
20
21
22
23
24
25
26
27
28
29
30
31
32
33
34
35
36
37
38
39
40
41
42
43
44
45
46
47
48
49

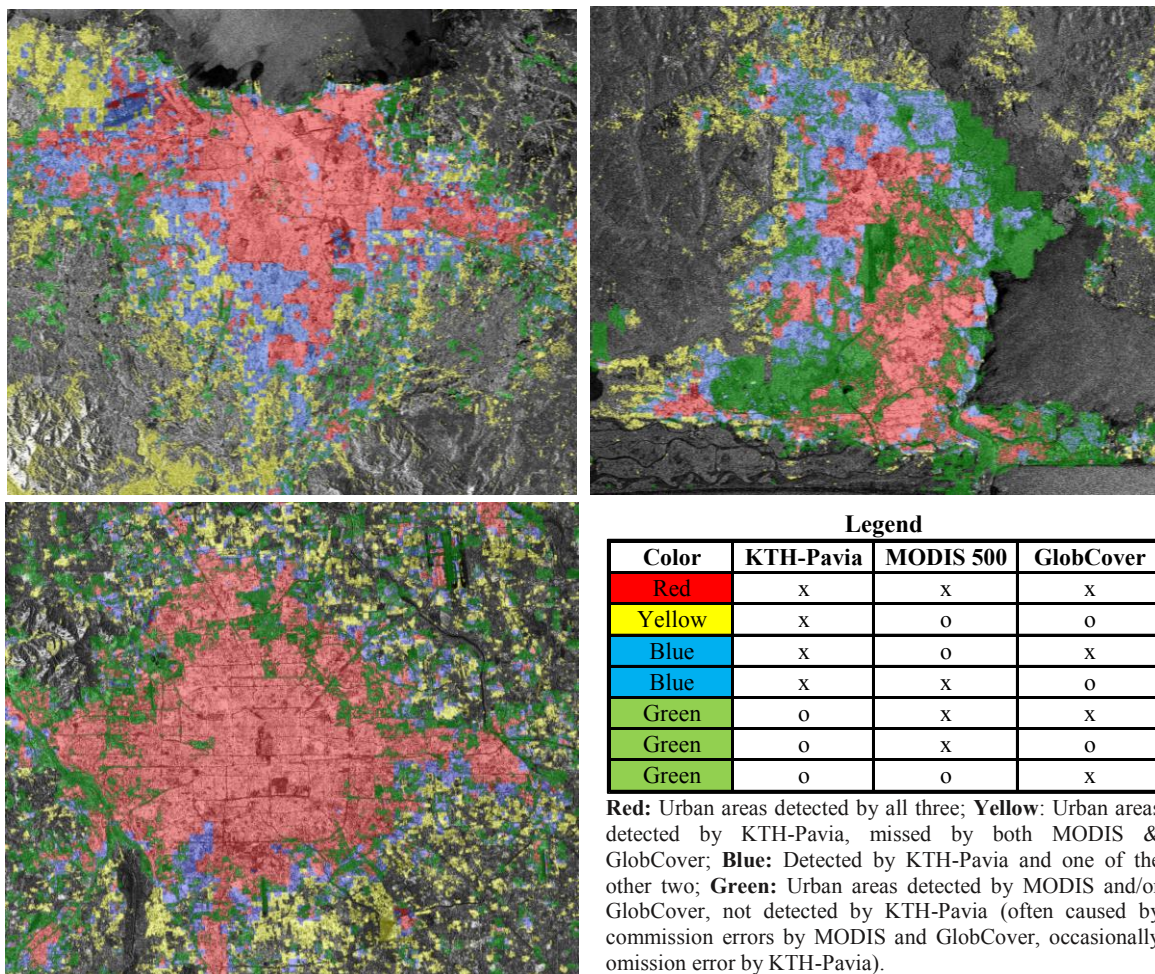
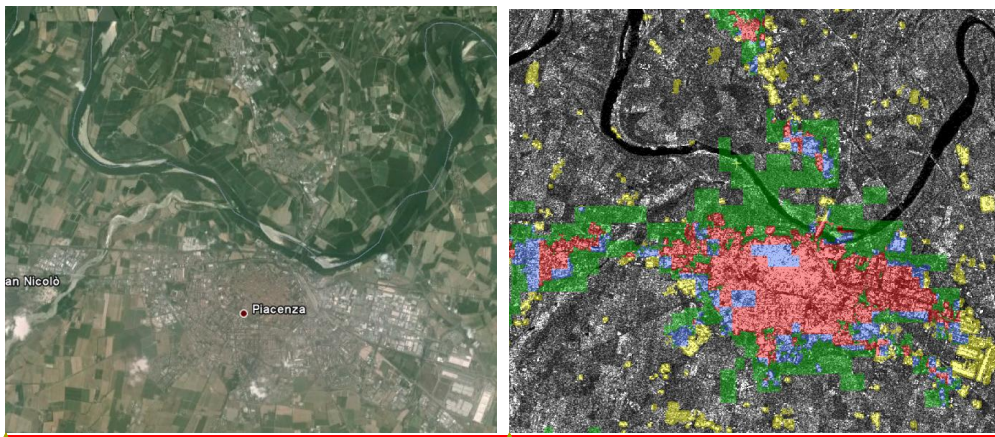


Figure 4. Overlay of KTH-Pavia Urban Extractions with MODIS 500m & GlobCover, Top: Jakarta, Center: Lagos; Bottom: Beijing,

Table 3: Accuracy Comparisons for Lombardia

Lombardia	Kappa	Overall Accuracy %	Urban Comission %	Urban Omission %
<u>KTH-Pavia ASAR Asc</u>	<u>0.66</u>	<u>82.59</u>	<u>3.49</u>	<u>31.11</u>
<u>KTH-Pavia ASAR Dsc</u>	<u>0.46</u>	<u>72.29</u>	<u>2.08</u>	<u>52.49</u>
<u>KTH-Pavia Asc & Dsc</u>	<u>0.83</u>	<u>91.33</u>	<u>1.36</u>	<u>15.58</u>
<u>MODIS 500</u>	<u>0.54</u>	<u>76.70</u>	<u>6.90</u>	<u>38.60</u>
<u>GlobCover</u>	<u>0.59</u>	<u>79.50</u>	<u>1.80</u>	<u>37.90</u>



Formatted: Font: (Default) Times New Roman, Font color: Custom Color(26,24,24)

Formatted: Font: (Default) Times New Roman, Font color: Custom Color(26,24,24)

Figure 5. Left: Google Image; Right: Overlay of KTH-Pavia Urban Extractions with MODIS 500m & GlobCover in Piacenza, Northern Italy (Legend is the same as Figure 4).

4.2 Effects of Contrast Enhancement

The results show that simple contract enhancement as described in section 3.2 could improve the urban extraction accuracies significantly as shown in Figure 65. It can be observed that the city center of Beijing including the Forbidden City and the Hutong areas with small houses (see the red rectangle in city center) were undetected using the original Pavia method (Fig. 65 left). After contrast enhancement, urban detection was very much improved (Fig. 65 right). Similar improved results were obtained for all other cities.

1
2
3
4
5
6
7
8
9
10
11
12
13
14
15
16
17
18
19
20
21
22
23
24
25
26
27
28
29
30
31
32
33
34
35
36
37
38
39
40
41
42
43
44
45
46
47
48
49
50
51
52
53
54
55
56
57
58
59
60
61
62
63
64
65



Figure 65. Beijing Result, Left: From the original Pavia method, Right Improved urban extraction using the contrast enhanced SAR data.

In addition, it is found that the whole image with enhancement produced significantly better results than a smaller subset with the original Pavia method as shown in Table 43 and Figure 76.

Two possible reasons for this, one is that the 2% cut off at the high end of the histogram may have removed the very bright urban pixels in the city center while the other is that it is more important to have at least an area with low backscatter in the scene to improve the overall contrast of the scene as in the case of New York where part of the image with water was clipped off to save computation initially.

Table 43. Comparison of Urban Extraction Accuracies in New York

	New York Urban Extraction	
	Subset Original	Whole Scene Enhanced
Kappa standard	0.13	0.77
Overall Accuracy	53%	88%
Urban Commission	0.00	4.05
Urban Omission	85.28	17.09

1
2
3
4
5
6
7
8
9
10
11
12
13
14
15
16
17
18
19
20
21
22
23
24
25
26
27
28
29
30
31
32
33
34
35
36
37
38
39
40
41
42
43
44
45
46
47
48
49
50
51
52
53
54
55
56
57
58
59
60
61
62
63
64
65

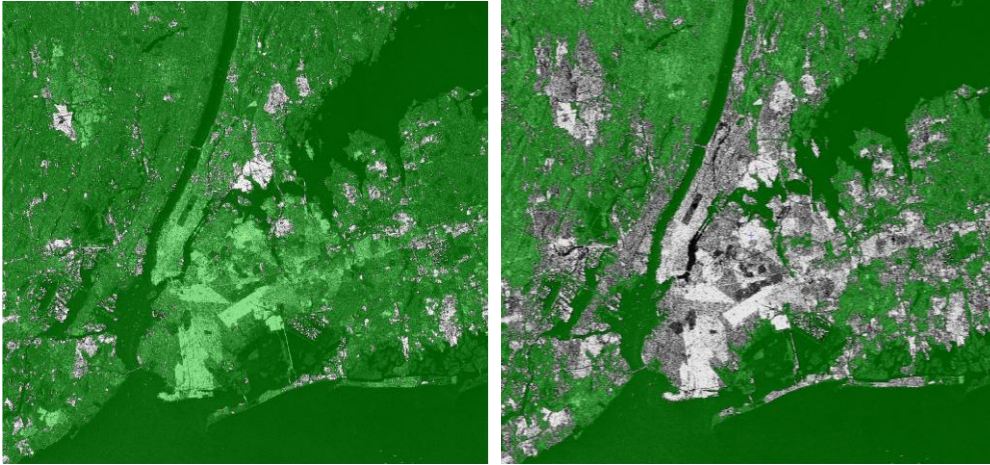


Figure 76. New York Urban Extractions, Left: From ASAR Subset using original Pavia method; Right: From Whole ASAR scene using KTH-Pavia Enhancement.

4.3 Effects of Mountain Masks

Using a mountain mask, mountains were effectively removed from urban extractions for Jakarta, Mumbai, and Rio and the commission errors reduced by approximately 2%, 7 % and 12% respectively (Table 5 . Figure 87).

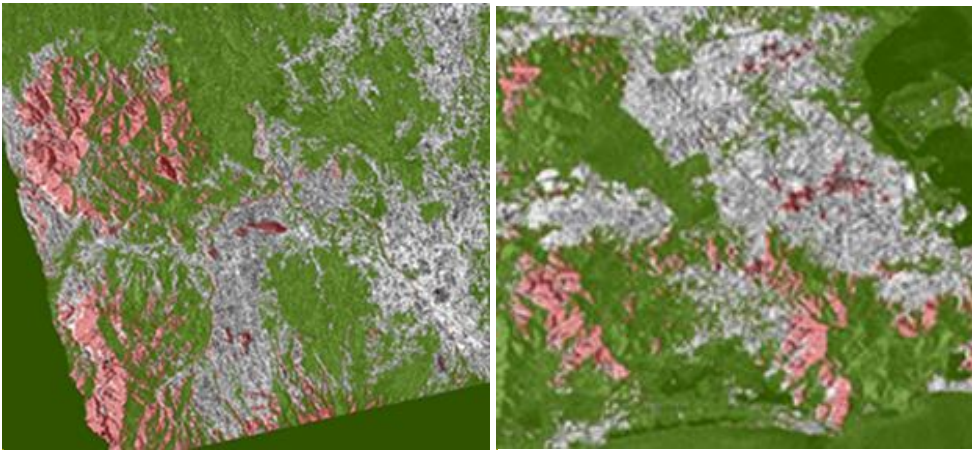


Figure 87. Commission errors removed with a mountain mask for Jakarta (Left) Mumbai, and Rio (Right).

Formatted: Font: (Default) Times New Roman, Font color: Custom Color(26,24,24)

Formatted: Font: (Default) Times New Roman, Font color: Custom Color(26,24,24)

1
2
3
4
5
6
7
8
9
10
11
12
13
14
15
16
17
18
19
20
21
22
23
24
25
26
27
28
29
30
31
32
33
34
35
36
37
38
39
40
41
42
43
44
45
46
47
48
49
50
51
52
53
54
55
56
57
58
59
60
61
62
63
64
65

Table 54. Comparison of Urban Extraction Accuracies with and without Mountain Mask

	Comparison with Mountain Mask (MM)					
	Jakarta	MM	Mumbai	MM	Rio	MM
Kappa	0,81	0,83	0,68	0,74	0,46	0,56
Overall Accuracy	91%	92%	84%	87%	73%	78%
Urban Commission	4,87	3,06	9,49	2,14	19,41	7,02
Urban Omission	15,15	15,15	23,03	23,03	39,84	39,84
Overall Accuracy Gain		0,79%		3,33%		4,94%
Commission Difference		-1,82		-7,35		-12,39

As rough water has higher backscatter than calm water and causes low contrast in the SAR images thus reduced urban detection, an attempt was also made to reduce the effects of rough water in Mumbai by clipping off the rough water pixels. The results show that kappa increased 17% while urban omission errors decreased significantly, from 45% to 23% (Table 65). Therefore, the development of water mask is underway using SRTM DEM where water has the lowest value that can be used as a mask.

Table 65. Comparison of Urban Extraction Accuracies with and without Rough Water

	Mumbai Results	
	Including rough water	Excluding rough water
Kappa	0,51	0,68
Overall Accuracy	76%	84%
Urban Commission	8,70	9,49
Urban Omission	45,28	23,03

4.4 Multitemporal Alternating-Polarization Dual Orbital SAR for Urban Extraction

Table 76 presents the urban extraction results from single-date single-polarization, single-date dual-polarization, combination of ascending and descending orbits, and the combination of all C-VV data. It is observed that single-data single polarization ASAR data from May 17 and May 27 could produce urban extraction with good accuracies. The extraction accuracies were further improved when two images were combined with a 3-7% improvement in kappa for C-HH and C-

VV combination and 11-20% improvement in kappa for the ascending and descending combination. These improvements were achieved mainly by reducing omission errors with the OR operator. The best results were achieved by using all four-date SAR in C-VV polarization, but the accuracy is only slightly higher than the ascending and descending combination. The results indicate that, using KTH-Pavia Urban Extractor, operational urban extraction is possible with two-date single-polarization SAR data from both ascending and descending orbits.

Table 7.6 Comparisons of Urban Extraction Accuracies from Multitemporal Alternating Polarization Dual-Orbit ASAR Data

Beijing	Kappa	Overall Accuracy %	Urban Commission %	Urban Omission %
May 17 VV IS2 Ascending (A)	0,68	84,02%	8,34%	25,07
May 17 HH IS2 Ascending	0,72	85,90%	2,34%	26,36
May 27 VV IS 2 Descending (D)	0,59	80,33%	7,20%	38,12
May 17 VV A OR May 27 D VV	0,79	89,49%	7,09%	16,58
May 17 VV OR HH A	0,75	87,72%	7,73%	17,60
June 8 A VV IS4	0,56	78,11%	3,94%	43,18
June 11 A VV IS6	0,57	78,70%	6,49%	40,14
All dates VV OR	0,79	89,63%	11,04%	11,67

5. Conclusions

This research develops a robust and operational method, KTH-Pavia Urban Extractor for global urban mapping using ENVISAT ASAR Data. ENVISAT ASAR C-VV data at 30m resolution were selected over 10 global cities and one rural area with smaller towns from six continents.

The results show that the KTH-Pavia Urban Extractor is effective in extracting urban areas at 30m resolution from a single-date single-polarization ENVISAT ASAR data with very good accuracies. When using two SAR images from C-HH and C-VV polarization, the extraction accuracy was further improved. The best accuracy was achieved using single-date single-

1
2
3
4
5
6
7
8
9
10 polarization SAR from both ascending and descending orbits. The results also demonstrated that
11 adding more multitemporal data only improve the urban extraction accuracy slightly. These
12 findings indicate that, with KTH-Pavia Urban Extractor, operational global urban mapping is
13 possible using very few well-selected spaceborne SAR images. With the recent launch of
14 Sentinel-1, C-band SAR data with global coverage became routinely available. Together with
15 historical ENVISAT ASAR and ERS-1/-2 SAR data, KTH-Pavia Urban Extractor can be used for
16 global urbanization monitoring in an efficient and reliable manner at low cost.

23 24 25 **Acknowledgement**

26
27 The research is part of the project ‘Urbanization and Climate Impact’ within the European Space
28 Agency (ESA) and Chinese Ministry of Science and Technology (MOST) Dragon 3 program.
29 The authors would like to thank ESA for the ENVISAT ASAR data. This research is supported
30 by a research grant from the Swedish National Space Board (PI: Yifang Ban).

31 32 33 34 35 36 37 **References**

- 38
39 Angiuli, E.; Trianni, G., 2014. Urban Mapping in Landsat Images Based on Normalized
40 Difference Spectral Vector, *IEEE Geoscience and Remote Sensing Letters*, vol.11, no.3,
41 pp.661,665.
- 42
43 Arino, O., J. Ramos, V. Kalogirou, P. Defourny, and F. Achard, “Globcover 2009,” in *Proc. ESA*
44 *Living Planet Symp.*, Bergen, Norway, 2010, pp. 686–689.
- 45
46 Ash, C., Jasny, B. R., Roberts, L., Stone, R. and Sugden, A. M., 2008. Reimagining Cities.
47 *Science* 319:739.
- 48
49 Ban, Y., H. Hu and I. Rangel, 2010. Fusion of QuickBird MS and RADARSAT-1 SAR Data for
50 Land-Cover Mapping: Object-based and Knowledge-Based Approach. *International Journal of*
51 *Remote Sensing*, 31(6):1391-1410.
- 52
53 Chen, J., Chen, J., Gong, P., Liao, A., He, C., 2011. Higher Resolution GLC Mapping. *Geomatics*
54 *World* 4 (2), 12-14.

1
2
3
4
5
6
7
8
9
10
11
12
13
14
15
16
17
18
19
20
21
22
23
24
25
26
27
28
29
30
31
32
33
34
35
36
37
38
39
40
41
42
43
44
45
46
47
48
49
50
51
52
53
54
55
56
57
58
59
60
61
62
63
64
65

Clausi, D. A., 2002. An analysis of co-occurrence texture statistics as a function of grey level quantization. *Can. J. Remote Sensing*, Vol. 28, No. 1, pp. 45–62.

Dell'Acqua, F., P. Gamba, and G. Lisini. 2003. "Improvements to Urban Area Characterization Using Multitemporal and Multiangle SAR Images." *IEEE Transactions on Geoscience and Remote Sensing* 41 (9): 1996–2004. doi:10.1109/TGRS.2003.814631.

Elvidge, C. D., Sutton, P. C., Tuttle, B. T., Ghosh, T. and Baugh, K. E., 2009. Global Urban Mapping Based on Nighttime Lights. In *Global Mapping of Human Settlement: Experiences, Datasets, and Prospects*. Gamba, P., and Herold, M., eds. Taylor and Francis Press.

[ESA and Array System Computing Inc, 2014. Nest User Manual 5.0, available online from: http://nest.s3.amazonaws.com/docs/nest_user_manual-5.0.pdf](http://nest.s3.amazonaws.com/docs/nest_user_manual-5.0.pdf), last accessed 2014-02-11.

Esch, T., M. Marconcini, A. Felbier, A. Roth, W. Heldens, M. Huber, M. Schwinger, H. Taubenbock, A. Muller, and S. Dech. 2013. "Urban Footprint Processor - Fully Automated Processing Chain Generating Settlement Masks From Global Data of the TanDEM-X Mission." *IEEE Geoscience and Remote Sensing Letters*: 1–5.

Esch, Thomas, Hannes Taubenböck, Achim Roth, Wieke Heldens, Andreas Felbier, Michael Thiel, Martin Schmidt, Andreas Müller, and Stefan Dech. 2012. "TanDEM-X Mission—new Perspectives for the Inventory and Monitoring of Global Settlement Patterns." *Journal of Applied Remote Sensing* 6 (1): 061702–1.

[Esch, T., M. Thiel, A. Schenk, A., Roth, A. Müller, S. Dech \(2010\): Delineation of Urban Footprints From TerraSAR-X Data by Analyzing Speckle Characteristics and Intensity Information, IEEE Transactions on Geoscience and Remote Sensing, Vol. 48, Issue 2, pp. 905-916](#)

Friedl, M.A., D. Sulla-Menashe, B. Tan, A. Schneider, N. Ramankutty, and A. Sibley, 2010. "MODIS collection 5 global land cover: Algorithm refinements and characterization of new datasets," *Remote Sens. Environment*, vol. 114, pp. 168–182.

Gamba P. and M. Stasolla, 2008. "Spatial indexes for the extraction of formal and informal human settlements from high resolution SAR images," *IEEE J. Special Topics Appl. Earth Observ. Remote Sens.*, vol. 1, pp. 98–106.

Gamba, P., and Herold, M. (Eds.). 2009. Global mapping of human settlements: Experiences, datasets, and prospects. Boca Raton, Florida, U.S.A: CRC Press.

1
2
3
4
5
6
7
8
9
10 Gamba, Paolo, Massimiliano Aldrichi, and Mattia Stasolla. 2011. "Robust Extraction of Urban
11 Area Extents in HR and VHR SAR Images." *IEEE Journal of Selected Topics in Applied Earth*
12 *Observations and Remote Sensing* 4 (1) (March): 27–34. doi:10.1109/JSTARS.2010.2052023.

13
14 Gamba, P., and G. Lisini. 2013. "Fast and Efficient Urban Extent Extraction Using ASAR Wide
15 Swath Mode Data." *IEEE Journal of Selected Topics in Applied Earth Observations and Remote*
16 *Sensing* Early Access Online. doi:10.1109/JSTARS.2012.2235410.

17
18 Giri, C., E. Ochieng, L. L. Tieszen, Z. Zhu, A. Singh, T. Loveland, J. Masek, and N. Duke. 2011.
19 "Status and Distribution of Mangrove Forests of the World Using Earth Observation Satellite
20 Data." *Global Ecology and Biogeography* 20: 154–9.

21 Griffiths, Patrick, Patrick Hostert, Oliver Gruebner, and Sebastian van der Linden. 2010.
22 "Mapping Megacity Growth with Multi-sensor Data." *Remote Sensing of Environment* 114 (2)
23 (February 15): 426–439. doi:10.1016/j.rse.2009.09.012.

24
25
26 Gong, P., Wang, J., Yu, L., Zhao, Y., Zhao, Y., Liang, L., Niu, Z., Huang, X., Fu, H., Liu, S., Li,
27 C., Li, X., Fu, W., Liu, C., Xu, Y., Wang, X., Cheng, Q., Hu, L., Yao, W., Zhang, H., Zhu, P.,
28 Zhao, Z., Zhang, H., Zheng, Y., Ji, L., Zhang, Y., Chen, H., Yan, A., Guo, J., Yu, L., Wang, L.,
29 Liu, X., Shi, T., Zhu, M., Chen, Y., Yang, G., Tang, P., Xu, B., Giri, C., Clinton, N., Zhu, Z.,
30 Chen, J., Chen, J., 2013. Finer resolution observation and monitoring of GLC: first mapping
31 results with Landsat TM and ETM+ data, *International Journal of Remote Sensing* 34 (7), 2607–
32 2654.

33
34
35 [Kemper T., Pesaresi M., Soille P., Guo H., Zanchetta L., Gueguen L., Blaes X., Ehrlich D., Lu L.,](#)
36 [Ferri S., Ouzounis G., Syrris V., Scavazzon M., Halkia S., 2013. A Global Human Settlement](#)
37 [Layer From Optical HR/VHR RS Data: Concept and First Results](#) *IEEE J. Sel. Topics Appl.*
38 [Earth Observ. Remote Sens., vol. 5, no. 6, pp. 2102 - 2131.](#)

39
40 Lu, Dengsheng, Hanqin Tian, Guomo Zhou, and Hongli Ge. 2008. "Regional Mapping of Human
41 Settlements in Southeastern China with Multisensor Remotely Sensed Data." *Remote Sensing of*
42 *Environment* 112 (9) (September 15): 3668–3679. doi:10.1016/j.rse.2008.05.009.

43
44 Moran, E. F., 2010. Land Cover Classification in a Complex Urban-Rural Landscape with
45 Quickbird Imagery. *Photogramm Eng Remote Sensing*. 2010 Oct;76(10):1159-1168.

46
47 Niu, X., and Y. Ban, 2013. Multitemporal RADARSAT-2 Polarimetric SAR Data for Urban
48 Land Cover Classification using Object-based Support Vector Machine and Rule-based
49 Approach, *International Journal of Remote Sensing*, 34(1):1-26.

50
51
52 Pesaresi, M, D. Ehrlich, I. Caravaggi, M. Kauffmann, and C. Louvrier, 2011. "Toward global
53 automatic built-up area recognition using optical VHR imagery," *IEEE J. Sel. Topics Appl. Earth*
54 *Observ. Remote Sens.*, vol. 4, no. 4, pp. 923–934.

1
2
3
4
5
6
7
8
9
10
11
12
13
14
15
16
17
18
19
20
21
22
23
24
25
26
27
28
29
30
31
32
33
34
35
36
37
38
39
40
41
42
43
44
45
46
47
48
49
50
51
52
53
54
55
56
57
58
59
60
61
62
63
64
65

Potere, David, Annemarie Schneider, Shlomo Angel, and Daniel Civco. 2009. "Mapping Urban Areas on a Global Scale: Which of the Eight Maps Now Available Is More Accurate?" *International Journal of Remote Sensing* 30 (24): 6531–6558. doi:10.1080/01431160903121134.

Schneider, A., M. A. Friedl, and D. Potere, "A new map of global urban extent from MODIS satellite data," *Environ. Res. Lett.*, vol. 4, no. 4. 2009.

Schneider, Annemarie, Mark A. Friedl, and David Potere. 2010. "Mapping Global Urban Areas Using MODIS 500-m Data: New Methods and Datasets Based on 'urban Ecoregions'." *Remote Sensing of Environment* 114 (8) (August 16): 1733–1746. doi:10.1016/j.rse.2010.03.003.

Seto, K. C., Fragkias, M., Güneralp, B., Reilly, M. K. "A meta-analysis of global urban land expansion." *PLoS ONE* 6.8 (2011): e23777.

Taubenböck, H., T. Esch, A. Felber, M. Wiesner, A. Roth, and S. Dech. 2012. "Monitoring Urbanization in Mega Cities from Space." *Remote Sensing of Environment* 117 (February): 162–176. doi:10.1016/j.rse.2011.09.015.

Thenkabail, P. S., C.M. Biradar, P. Noojipady, V. Dheeravath, Y. J. Li, M. Velpuri, M. Gumma, G. P. O. Reddy, H. Turrall, X. L. Cai, J. Vithanage, M. Schull, and R. Dutta. 2009. "Global Irrigated Area Map (GIAM), Derived From Remote Sensing, for the End of the Last Millennium." *International Journal of Remote Sensing* 30: 3679–733.

Townshend, J. R. G., J. G. Masek, C. Q. Huang, E. F. Vermote, F. Gao, S. Channan, S. Jo, M. Feng, R. Narasimhan, D. Kim, K. Song, D. X. Song, X. P. Song, P. Noojipady, B. Tan, M. C. Hansen, M. X. Li, and R. E. Wolfe. 2012. "Global Characterization and Monitoring of Forest Cover Using Landsat Data: Opportunities and Challenges." *International Journal of Digital Earth* 5: 373–97.

UN (United Nations) 2011. *World Urbanization Prospects: The 2011 Revision*. Population Division of the Department of Economic and Social Affairs of the United Nations Secretariat <http://esa.un.org/unup>.

Wang, L., P. Gong, Q. Ying, Z. Yang, X. Cheng, and Q. Ran. 2010. "Settlement Extraction Over North China Plain with Landsat and Beijing-1 Data Using an Improved Watershed Segmentation Algorithm." *International Journal of Remote Sensing* 31: 1411–26.

Wang L., C. Li, Q. Ying, X. Cheng, X. Wang, X. Li, L. Hu, L. Liang, L. Yu, H. Huang, P. Gong. 2012. China's Urban Expansion from 1990 to 2010 Determined with Satellite Remote Sensing. *Chinese Science Bulletin*, 57(22):2802-2812.

1
2
3
4
5
6
7
8
9
10
11
12
13
14
15
16
17
18
19
20
21
22
23
24
25
26
27
28
29
30
31
32
33
34
35
36
37
38
39
40
41
42
43
44
45
46
47
48
49
50
51
52
53
54
55
56
57
58
59
60
61
62
63
64
65

Zhang, Qingling, and Karen C. Seto. 2011. "Mapping Urbanization Dynamics at Regional and Global Scales Using Multi-temporal DMSP/OLS Nighttime Light Data." *Remote Sensing of Environment* 115 (9) (September 15): 2320–2329. doi:10.1016/j.rse.2011.04.032.

